AIAA SciTech Forum
9 - 13 January 2017, Grapevine, Texas
58th AIAA/ASCE/AHS/ASC Structures, Structural Dynamics, and Materials Conference

10.2514/6.2017-0405

High-Speed Vehicle Fluid-Structure-Jet Interaction Analysis and Modeling

Ryan C. Kitson[*] and Carlos E. S. Cesnik[†]

University of Michigan, Ann Arbor, MI, 48109, USA

This paper presents high-fidelity solutions of the fluid-structure-jet interaction problem for slender high-speed vehicles along with two jet interaction modeling methods, one semi-empirical and one CFD-based, to approximate the high-fidelity solution. The high-fidelity solutions of a representative high-speed vehicle with jet interaction and structural deformation show that the resultant loads are affected by the deformation. The semi-empirical jet interaction model is developed using previous work in the literature and approximates the main features of the jet interaction solution when compared to numerical and experimental results. The CFD-based jet interaction model is developed by using data-fusion of a previously developed aerodynamic loads surrogate, the semi-empirical jet interaction model, and CFD solutions of the jet interaction. This data-fusion model approximates the surface pressure of a representative high-speed vehicle with varying flow, structure, and jet parameters and can be used within a flight simulation framework. Overall, the work demonstrates a need to model the fluid-structure-jet interaction of high-speed vehicles and modeling methods that may be used to approximate the full solution.

Nomenclature

AoA	Angle of attack, deg
C	Speed of sound, m/s
E	Energy per unit length of the jet, J/m
J_0	Blast wave constant
M_∞	Free-stream Mach number
PR	Ratio of jet total pressure to free-stream static pressure
R	Shock front distance from the blast origin, m
R_0	Blast characteristic length, m
T	Temperature, K
U	Wave propagation velocity, m/s
V_∞	Free-stream velocity, m/s
X	Training points for the co-Kriging model
Y	SVD modal amplitudes at the training points for the co-Kriging model
Z	Gaussian process
b_e	Jet nozzle exit diameter, m
h	Height of the equivalent forward facing step due to jet interaction, m
h_s	Jet terminal shock height in the free-stream, m
p_b	Back pressure behind the jet, Pa
p_c	Matrix of surface pressures from the aerodynamic surrogate model
p_e	Jet exit pressure, Pa
p_e	Matrix of surface pressures from the CFD JI solution
p_{0a}	Attitude jet total pressure, Pa
p_{0d}	Divert jet total pressure, Pa

---

[*]Ph.D. Candidate, Department of Aerospace Engineering, kitson@umich.edu; AIAA Student Member
[†]Professor, Department of Aerospace Engineering, cesnik@umich.edu; AIAA Fellow

p_∞	Free-stream static pressure, Pa
p_{p_1}	First plateau pressure due to a forward facing step, Pa
p_{p_2}	Second plateau pressure due to a forward facing step, Pa
t	Time, s
x	Downstream distance from the jet, m
$x^{(n+1)}$	Co-Kriging next evaluation point
x_s	Oblique shock location due to boundary layer separation, m
y	Co-Kriging approximation
Ψ	Correlation function
α_s	Deflection angle required to achieve the pressure ratio p_{p_1}/p_∞, rad
γ_e	Jet exit ratio of specific heats
μ	Process mean
ρ_z	Co-Kriging tuning parameter
σ^2	Process variance

Subscripts

∞	Free-stream quantity
0	Flow total quantity
c	Cheap function quantity
d	Difference of the cheap and expensive functions quantity
e	Expensive function quantity
ij	Matrix row and column indexes
j	Jet quantity

I.   Introduction

MANEUVERABLE high speed vehicles may require large angles of attack for aggressive maneuvers as well as quick attitude changes during the final phase of flight. Attitude control jets can be effective at high angles of attack and have fast response times on the order of milliseconds.[1,2] The jet interaction with the oncoming flow adds a complex flow structure that can amplify or reverse the applied forces.[3] However, slender high speed vehicles have added flexibility that will lead to fluid-structure interaction due to larger structural deformations under large aerodynamic loads. On a flexible vehicle there could be fluid-structure-jet interactions that can affect the response and stability of the system.

The effect of fluid-structure-jet interactions (FSJI) has yet to be understood for either a fixed structure or free vehicle. Previous work on the jet interaction (JI) with the oncoming supersonic flow has shown a characteristic flow structure that develops around the jet exit and is sensitive to the flow and jet variables. Roger[3] summarized a large number of experimental and computational works on jet interaction that showed the lateral force amplification factor on the body can be negative, which would result in control reversal. This implies there is a parameter space of fluid, structure, and jet variables for control reversal that would need to be modeled prior to control design.

In addition to a wide range of parameters that affect the jet interaction solution, the method used to analyze the problem can also influence the solution. DeSpirito[4] completed a study using experimental data of a flat plate with a jet-in-crossflow to study the effect of turbulence modeling on the solution. Each turbulence model led to a different solution with varying levels of accuracy relative to the experimental solution. One specific turbulence model did not prove to be the best for each test case, which further emphasizes the sensitivity of the solution to turbulence modeling. Ferrante et al.[5] used a Large Eddy Simulation (LES) approach to study the jet interaction of an inclined jet to capture the vortex shedding, shear layer and barrel shock among other jet interaction features. However, despite capturing these effects one major conclusion was that the turbulence level of the inflow conditions had a significant impact on the solution. The computational studies of jet interaction have shown that it is possible to match the experimental conditions, but it is difficult to know what computational method is suitable *a priori*. In addition, these methods are computationally expensive and would be prohibitive for studying early design iterations of a vehicle. Empirical[6] and theoretical[7–9] models have been used in the past to model jet interaction, but these are either restricted to two dimensional solutions or have not been extensively verified against experimental data. Developing a reduced order model for three dimensional jet interactions would reduce the computational cost while capturing the important features in the flow.

American Institute of Aeronautics and Astronautics

Sahu et al.[10] and VanderWyst et al.[11] both used computational fluid dynamics (CFD) solutions to create a reduced model of the slender high speed vehicle surface loads due to aerodynamics and jet interaction. Sahu et al.[10] went on to use this reduced model in a coupled rigid-body dynamics (RBD) simulation and compared the results to a coupled CFD/RBD solution. The two solutions in terms of vehicle loading and attitude are very similar when the vehicle is stabilized by a high initial roll rate. Overall, this method demonstrates how the aerodynamic and jet interaction forces can be modeled successfully without CFD in the loop. VanderWyst et al.[11] also used a selection of CFD samples to create a reduced order model and present the sampling, verification, and validation procedures necessary to build a quality and reliable model. This work highlights the expense and difficulty associated with high speed vehicles that can have many degrees of freedom such as multiple jets, articulated control surfaces, and a wide range of flight conditions. These works demonstrated the capability to balance accuracy and computational expense by using limited CFD solutions, but did not address the additional degrees of freedom associated with structural deformation. The additional structural degrees of freedom add several more dimensions to the reduced model and could lead to a large increase in sample CFD runs.

This paper presents the development of a semi-empirical and CFD-based jet interaction modeling approach that can be used to study FSJIs on a representative flexible high speed vehicle. The CFD-based model uses CFD solutions of the vehicle with and without the jet interaction using a data-fusion technique known as co-Kriging[12, 13] along with the semi-empirical jet interaction model. The data-fusion model can then be used without CFD in the loop to simulate the vehicle loads at various flow conditions, structural deformations, and jet conditions. The numerical results begin with the high-fidelity solution of a representative high-speed vehicle with jet interaction, structural deformation. These results show the trends and parameters that need to be considered when building a model of the jet interaction solution for slender and agile vehicles. The semi-empirical jet interaction model is then compared to numerical and experimental solutions of a flat plate with jet-in-crossflow to demonstrate the ability to predict the pressure distribution due to jet interaction. Finally, the data-fusion model is compared to the CFD solution using a leave-one-out approach to measure the quality of the model and the ability to approximate the vehicle surface pressure distribution with limited degrees of freedom.

II.   Methods

Multiple modeling methods for approximating the jet interaction with a supersonic cross-flow are presented. First, a semi-empirical jet interaction model that approximates pressure distribution along a surface for range of fluid and jet parameters. Second, a CFD-based loads model that leverages the semi-empirical model, an aerodynamics surrogate model, and CFD solutions using a data-fusion approach. The data-fusion model is modeling approach that is being developed for the representative high-speed vehicle flight simulations. This approach expedites the modeling of the large parameter space of fluid, structure, and jet conditions for the high-speed maneuverable vehicle.

A.   Semi-Empirical Jet Interaction Model

The semi-empirical jet interaction model is based on empirical and theoretical representations of the jet interaction with a supersonic cross-flow. It is used to provide a fundamental understanding of the problem with minimal computational cost.

The reaction control system of the high-speed vehicle consists of multiple jets around the circumference of the vehicle nose that exhausts from the body surface perpendicular to the oncoming supersonic flow. The effective force on the vehicle is a combination of the aerodynamic force without the jet, the force applied from the momentum transfer at the jet nozzle, as well as the jet interaction that causes regions of higher pressure fore and lower pressure aft of the nozzle. Within the simulation framework the aerodynamic loads are solved for based on the current fluid and structural states. The jet interaction problem is solved for a value p/p_1 where p_1 is the pressure due to aerodynamic loading only and p is the pressure due to jet interaction. This factor is then used to calculate the final pressure distribution along the surface at the current time step.

The jet interaction model in the stream-wise direction is based on the work by Werle, Driftmyer and Shaffer.[6] The first area to be modeled is the boundary layer separation region ahead of the jet. This area has a very similar pressure profile to a forward-facing step that characteristically has two plateau pressures.

American Institute of Aeronautics and Astronautics

The first plateau pressure can be approximated by

$$p_{p_1} = (M_\infty/2 + 1)p_\infty \tag{1}$$

according to Zukoski[14] and the second plateau pressure can be approximated by

$$p_{p_2} = 1.3(p_{p_1} - p_\infty) + p_\infty. \tag{2}$$

Then, the back pressure p_b is approximately equal to p_{p_2}. With the back pressure, flow, and jet conditions the height of the jet terminal shock in the free-stream can be calculated by

$$h_s/b_e = 0.7(\gamma_e M_e^2 p_e/p_b)^{1/2} \tag{3}$$

where h_s is the height of the jet terminal shock in the free-stream, b_e is the jet exit diameter, and γ_e, M_e, p_e are the ratio of specific heats, Mach number, and pressure at the jet nozzle exit, respectively.

The height of the of jet terminal shock, h_s is used to calculate the equivalent step height h by

$$h = 1.36(h_s) \tag{4}$$

and the location of the oblique shock in front of the jet x_s is calculated using the step height h as

$$x_s = h/\tan\alpha_s \tag{5}$$

where the angle α_s is the deflection angle required to achieve the pressure ratio p_{p_1}/p_∞.

Once the shock location x_s and jet terminal shock height h_s have been calculated, the pressure profile ahead of the jet can be approximated by the profile shown in Figure 1. Similarly, the region behind the shock in the flow-straightening region can be approximated by the profile shown in Figure 2.
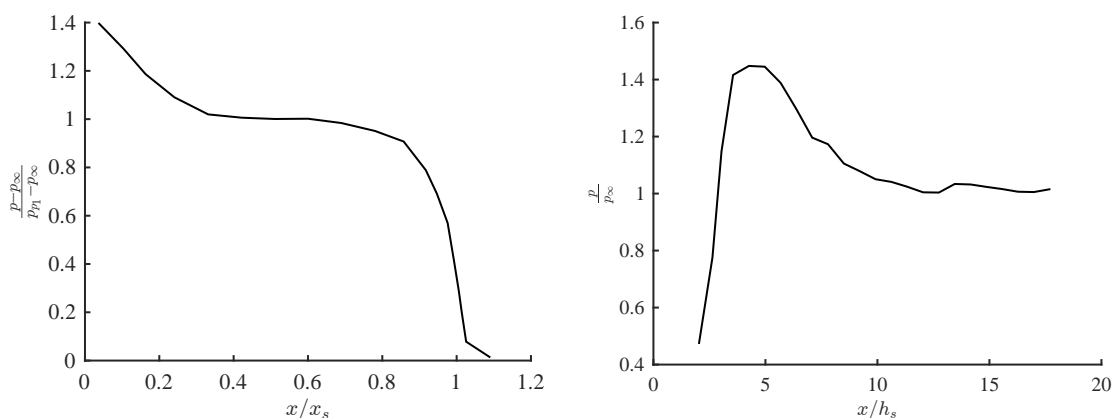
Figure 1. Pressure profile ahead of the jet based on empirical data

Figure 2. Pressure profile behind the jet in the flow-straightening region

The lateral jet interaction pressure profile is based on the analysis regarding blast waves and applied to a wave in a supersonic flow. The distance of the shock front is represented in terms of C, the speed of sound in the free-stream, U, the propagation velocity, R_0 a characteristic length based on the energy of the blast, and the constant J_0, which is a function of the ratio of specific heats and the dimensionality of the problem. The shock front distance R is represented by

$$\left(\frac{C}{U}\right)^2 \left(\frac{R_0}{R}\right)^3 = J_0 \tag{6}$$

for a spherical blast wave according to Sakurai.[7]

Following the work of Broadwell,[9] the propagation velocity U is rewritten as $\frac{dR}{dt}$. Solving for R yields

$$R = \left(\frac{C^2 R_0^3}{J_0}\right)^{1/6} (2t)^{1/2} \tag{7}$$

American Institute of Aeronautics and Astronautics

where t is expressed as x/V_∞, i.e., the distance downstream of the shock front over the free-stream velocity.

The constant J_0, for specific heat ratio $\gamma = 1.4$, and a spherical shock wave is equal to 0.596 according to the calculations by Sakurai.[8] The characteristic distance R_0 is calculated according to the cylindrical form of Broadwell[9] as

$$R_0 = \sqrt{E/(2\pi p_\infty)} \tag{8}$$

where E is the energy per unit length of the jet.

The shock front as a function of position defines the boundary of the stream-wise jet interaction model. Outside of the boundary a pressure profile that is the same as the forward-facing step profile is used. To calculate the profile at each span-wise point along the shock front, the first plateau pressure is defined as 10/13 times the pressure within the shock front at that chord-wise station.

B. CFD-Based Reduced Order Modeling of Jet Interaction

A reduced order model of the jet interaction is developed using a CFD-based surrogate model for aerodynamic loads, the semi-empirical jet interaction model, and the high-fidelity RANS CFD solution of the vehicle with jet interaction. This approach leverages the fundamental understanding from the aerodynamics-only surrogate model that was developed by Zettl *et al.*[15] and the semi-empirical jet interaction model that has been developed in this work. These solutions are then augmented by the prediction with CFD solutions of the jet interaction using the co-Kriging method. In this study, both the CFD-based surrogate and additional jet interaction CFD solutions used the NASA FUN3D CFD code[16] to solve the Reynolds-averaged Navier–Stokes equations with the Spalart–Allmaras one-equation turbulence model.

In the literature regarding co-Kriging there is generally a *cheap* function that is inexpensive to sample, but approximates an *expensive* function of interest that is sparsely sampled. The surrogate model of Zettl *et al.* in conjunction with the semi-empirical jet interaction model represents the *cheap* function in this work as the models have already been completed, but approximates the full jet interaction solution. Therefore, the additional jet interaction CFD solutions represent the *expensive* function of interest.

The jet interaction data-fusion model predicts the surface pressure of the vehicle for varying flight conditions, structural deformations, and jet conditions. These input conditions are grouped by discipline and listed in Table 1, where F refers to the fluid parameters, S the structural parameters, and J the jet parameters. The surrogate model of the aerodynamic loads takes the F and S parameters as inputs and outputs the pressure due to aerodynamic loads along the vehicle surface. The jet interaction model takes the F and J parameters as inputs and outputs the pressure ratio of jet interaction to aerodynamic solutions. The total *cheap* pressure distribution, p_c, is the combined solution from the aerodynamic surrogate and semi-empirical jet interaction model. The full set of F, S, and J parameters are used as inputs to the CFD solver to calculate the surface pressure distribution, p_e.

Table 1. **Input parameters for the CFD solver and co-Kriging model**

Category	Parameter
Fluid, F	Mach Number
	Angle of Attack
Structure, S	Structural Mode Amplitudes
Jet, J	Attitude jet total pressure, p_{0a}
	Divert jet total pressure, p_{0d}

The vehicle surface pressure is described in terms of orthogonal vectors and the predicted coefficients of each vector are then used to reconstruct the surface pressure due to jet interaction. The co-Kriging inputs are the F, S, and J parameters and the outputs are the m coefficients of the orthogonal vectors in the surface mesh N-dimensional space, where N is number of cells on the surface mesh and m is the number of orthogonal vectors. The singular value decomposition (SVD) is used to calculate the orthogonal vectors and then truncated to retain the m vectors with the most energy. First, two matrices are created for the cheap solution and the jet interaction CFD solution. The cheap model and CFD solution matrices are,

$$p_{c,ij} = p_c(x_i, y_i, z_i, F_j, S_j, J_j)$$
$$p_{e,ij} = p_e(x_i, y_i, z_i, F_j, S_j, J_j)$$

American Institute of Aeronautics and Astronautics

where p_c refers to the pressure distribution of the *cheap* CFD surrogate aerodynamic model combined with the semi-empirical JI model and p_e refers to the *expensive* CFD solution of the jet interaction.

Taking the SVD of the matrix p_e yields the orthogonal basis U_e, singular values Σ_e and orthogonal basis V_e where $p_e V_e = U_e \Sigma_e$. The singular values represent the energy associated with each vector and the number of vectors kept is determined when a specified amount of the total energy is retained. This process is related to the proper orthogonal decomposition of the matrix p_e where the matrix of basis vectors Ξ is equal to the retained vectors of $U_e \Sigma_e$ and the coefficients are equal to the retained rows of V_e. In this case all of the singular values are retained. Each row of V_e represents the coefficients at each set of expensive F, S, and J conditions. Therefore, if the coefficients of one column of V_e^T can be predicted at alternate input conditions as $\hat{\nu}$, an approximation of the surface pressure is $\hat{p} = \Xi \hat{\nu}$. The corresponding amplitudes of the Ξ basis vectors from the cheap solution V_c^T are calculated by

$$U_e S_e V_c^T = p_c \tag{9}$$

$$S_e V_c^T = U_e^T p_c \tag{10}$$

$$V_c^T = S_e^{-1} U_e^T p_c \tag{11}$$

For the co-Kriging approximation the inputs (X) and outputs (Y) are expressed as

$$X = \begin{bmatrix} X_c \\ X_e \end{bmatrix} = \begin{bmatrix} F_c, S_c, J_c \\ F_e, S_e, J_e \end{bmatrix}$$

$$Y = \begin{bmatrix} Y_c \\ Y_e \end{bmatrix} = \begin{bmatrix} V_e \\ V_c \end{bmatrix}$$

The co-Kriging approximation follows the work of Forrester *et al.*[12] and Kennedy and O'Hagan[13] where the value of the expensive function is the sum of the Gaussian process Z_d of the difference between cheap and expensive functions and ρ_z times the Gaussian process of the cheap function Z_c, i.e.,

$$Z_e(x) = \rho_z Z_c(x) + Z_d(x) \tag{12}$$

Using this form the co-Kriging approximation of the expensive function in the jth dimension y_{ej} given inputs $X = \{X_c, X_e\}^T$ and calculated outputs $Y = \{Y_c, Y_e\}^T$ is

$$\hat{y}_{ej}(x^{(n+1)}) = \hat{\mu} + c^T C^{-1}(Y_j - \mathbf{1}\hat{\mu}), \tag{13}$$

where $\mathbf{1}$ is a $n \times 1$ column vector of ones,

$$c = \left\{ \begin{array}{c} \rho_z \sigma_c^2 \psi_c(X_c, x^{(n+1)}) \\ \rho_z^2 \sigma_c^2 \psi_c(X_e, x^{(n+1)}) + \sigma_d^2 \psi_d(X_e, x^{(n+1)}) \end{array} \right\}, \tag{14}$$

$$C = \begin{bmatrix} \sigma_c^2 \Psi_c(X_c, X_c) & \rho_z \sigma_c^2 \Psi_c(X_c, X_e) \\ \rho_z \sigma_c^2 \Psi_c(X_e, X_c) & \rho_z^2 \sigma_c^2 \Psi_c(X_e, X_e) + \sigma_d^2 \Psi_d(X_e, X_e) \end{bmatrix}, \tag{15}$$

and $\hat{\mu} = \mathbf{1}^T C^{-1} y_{ej} / \mathbf{1}^T C^{-1} \mathbf{1}$. The variance of each function is σ^2 and ψ and Ψ are vectors and matrices, respectively, of the correlation functions. The subscripts c, d, and e refer to the *cheap*, *difference* and *expensive* functions, respectively.

The process for finding an optimal value of ρ_z can expand very quickly depending on the dimension of the output. To mitigate this computational cost, this work first creates a kriging model of the cheap training data with a polynomial regression function and Gaussian correlation function. The cheap approximation at the expensive training input data $\hat{Y}_c(X_e)$ is then calculated. As opposed to solving an optimization problem, the parameter ρ_z is calculated by

$$\rho_z = \frac{\hat{Y}_c(X_e)^T Y_e}{\|\hat{Y}_c(X_e)\| \|Y_e\|} \tag{16}$$

and the difference Y_d as

$$Y_d = Y_e - \hat{Y}_c(X_e) \rho_z \tag{17}$$

Finally, a second kriging is created using the expensive training input data and Y_d using polynomial regression and Gaussian correlation functions.

Figure 3 provides a block diagram of the full jet interaction modeling process in the pre-processing block. The simulation block of Figure 3 shows how an arbitrary set of fluid, structure, and jet parameters during simulation is collected into the set $\hat{X}$ for the co-Kriging model to approximate the amplitudes of the SVD vectors. Then, the approximated amplitudes, $\hat{\nu}$, are used with the basis set Ξ to calculate the approximate pressure distribution on the vehicle surface $\hat{p}$.
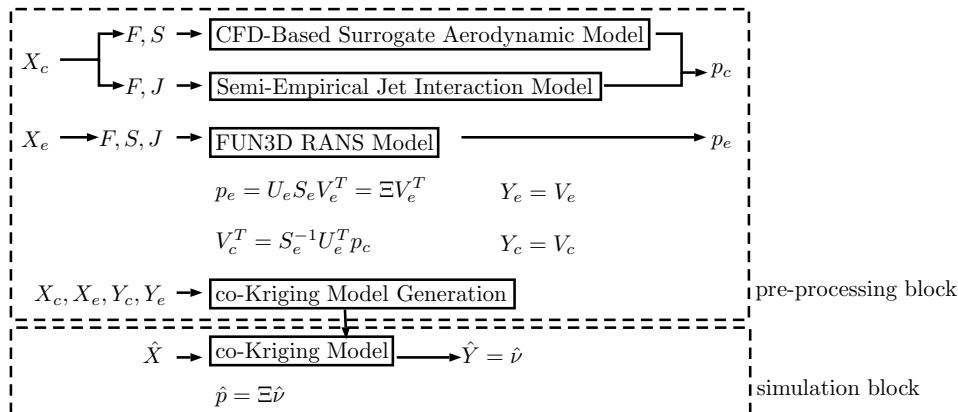
Figure 3. Block diagram of the jet interaction modeling process

III.   Numerical Modeling

A vehicle representative of slender high speed maneuverable vehicles is used for this study that was previously developed by Kitson and Cesnik.[17] The basic dimensions and flight conditions for the vehicle are shown in Table 2 and are inspired by existing vehicles, such as the Sidewinder and AMRAAM. The outer mold line of the model, shown in Figure 4, was chosen to move the center of pressure aft of the center of gravity based on the lack of fin surfaces that are conventionally located at the tail end of the vehicle. Markers for the center of pressure (C.P.) and center of gravity (C.G.) have been added to the figure based on the results of the baseline vehicle. Conventional fin surfaces are not included in this model due to their loss of effectiveness at high angles of attack. Instead, a divert and attitude control system of jets perpendicular to the surface is located at 25% and 50% of the vehicle length. This system is assumed to be composed of jets that provide additional forces normal to the body surface to control the vehicle orientation. The baseline configuration has a uniform mass and stiffness distributions, therefore the free-free vibration mode shapes in Figure 5 are similar to a uniform free-free beam.

Table 2. Basic properties and flight conditions for the vehicle

Property	Value	Unit
Total mass (uniform distribution)	85	kg
Length, L_{ref}	3	m
Diameter at mid-length	0.13	m
Reference Area, S_{ref}	0.39	m^2
Mach	2–4	
Reynolds number	38×10^6	
Altitude	50,000	ft

Regarding the CFD modeling and analysis the computational domain was created using Pointwise® and solved with the NASA FUN3D CFD code.[16] The code was used to solve the Reynolds-averaged Navier-Stokes equations with the Spalart–Allmaras (SA) turbulence model for the vehicle at various flow conditions.
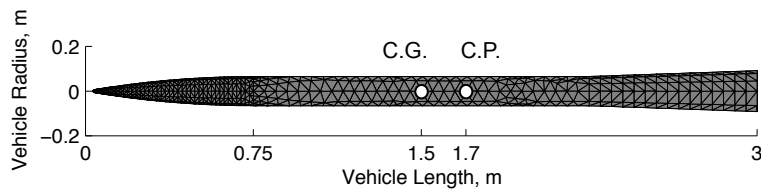
American Institute of Aeronautics and Astronautics

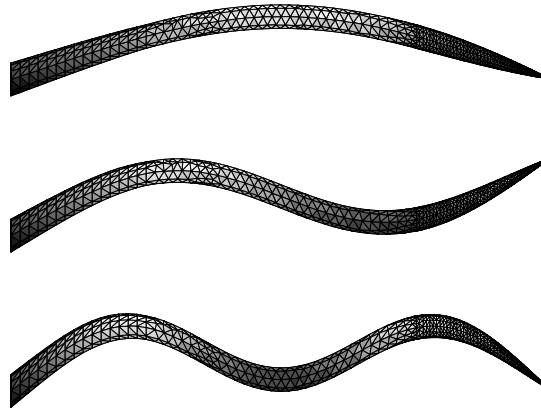**Figure 4. Side view of the undeformed axisymmetric vehicle**

Figure 5. Free-free vibration mode shapes of the vehicle with uniform mass and stiffness distributions

The computational domain for the grid convergence study is shown in Figure 6. The test conditions used were Mach 3 flow, 30 degrees AoA, no structural deformation, and PR 1500 for the attitude and divert jets. The results are presented in Figure 7 for the axial force, normal force, and pitch moment coefficients along with the relative error of each grid based on Richardson extrapolation for zero grid spacing. Approximately 5.3 million points were used in the entire domain with about 4.6 million points clustered around the vehicle. A wall spacing of 1×10^{-6}m was used to ensure a $y+$ value less than 1. The Roe scheme and the van Leer limiter augmented with a heuristic pressure limiter was used to solve for the convective fluxes. An implicit time-stepping method is used to converge to the steady-state solution with a CFL number ramped to 50 for the inviscid calculation and RANS calculation.

Table 3. Parameters and limits used for CFD jet interaction sampling

Category	Parameter	Lower Bound	Upper Bound	Units
Fluid, F	Altitude	50,000		ft
	Mach Number	2	4	
	Angle of Attack	-75	75	deg
Structure, S	First bending mode amplitude (longitudinal plane)	-5%	5%	L_{ref}
Jet, J	Attitude jet total pressure, p_{0a} (flow in $-z$ direction)	2.2×10^4	3.5×10^7	Pa
	Divert jet total pressure, p_{0d} (flow in $-z$ direction)	2.2×10^4	3.5×10^7	Pa
	Jet total temperature, T_0	2700		K

The data-fusion model is based on the understanding provided by the aerodynamic surrogate model and fundamental jet interaction model. This fundamental basis is then augmented with the high-fidelity CFD solutions of the vehicle at different flow, structure and jet conditions. The inputs to the jet interaction
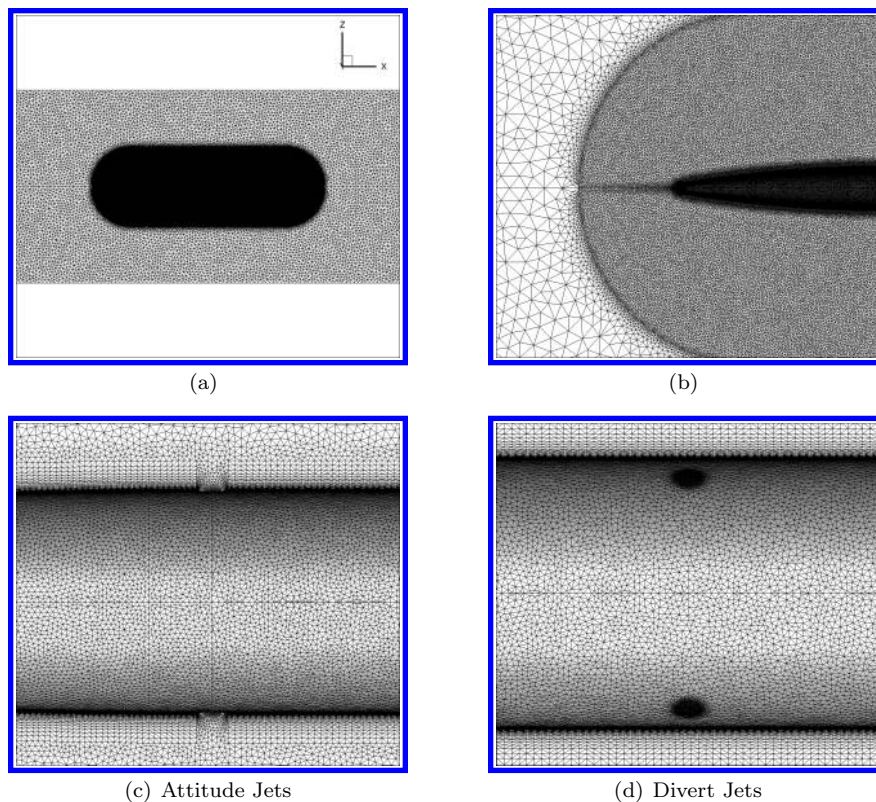
American Institute of Aeronautics and Astronautics

(a)

(b)

(c) Attitude Jets

(d) Divert Jets

Figure 6. Computational domain used for the vehicle CFD calculations

co-Kriging model are the F, S, and J parameters discussed in Section II and the parameter bounds for the CFD solutions were chosen based on previous flight simulation results by Kitson and Cesnik[17] shown in Table 3.

IV. Numerical Results

First, the high-fidelity solutions to the jet interaction problem are presented with high angles of attack and moderate structural deformation, which are characteristics of interest for the slender high-speed vehicle. The force coefficients and the amplification factors are selected to show the degree to which the jet interaction will have an effect in the steady state solution. Second, the jet interaction model development is presented using the data-fusion and surface domain methodology presented in the previous sections. The ability of the model to approximate the vehicle surface pressure distribution is presented, which is critical to future aeroelastic analysis.

A. High-Fidelity Jet Interaction Solutions with High Angles of Attack and Structural Deformation

Figure 8 shows the CFD solution of the vehicle with the attitude or divert jets on and at either positive or negative 45 degrees AoA. The normal force coefficient, pitch moment coefficient, and the corresponding amplification factors are presented in Figure 9. The moment amplification for the attitude jet initially increases with AoA up to approximately 1.4 until an AoA of approximately 20 degrees. Beyond this AoA, there is a reduction in control effectiveness, that is the force and moment amplification factors of the attitude and divert jets decrease below 1 for high angles of attack. The contour plots in Figure 8 show a large expansion region that occurs at high angles of attack that acts in the opposite direction of the applied jet thrust. The jet interaction due to the divert jets has an effect on the pitch moment, but it does not have a moment amplification factor because the location coincides with the center of mass.

Figure 10 shows the CFD solution of the jet interaction problem with positive or negative 5% tip bending

American Institute of Aeronautics and Astronautics
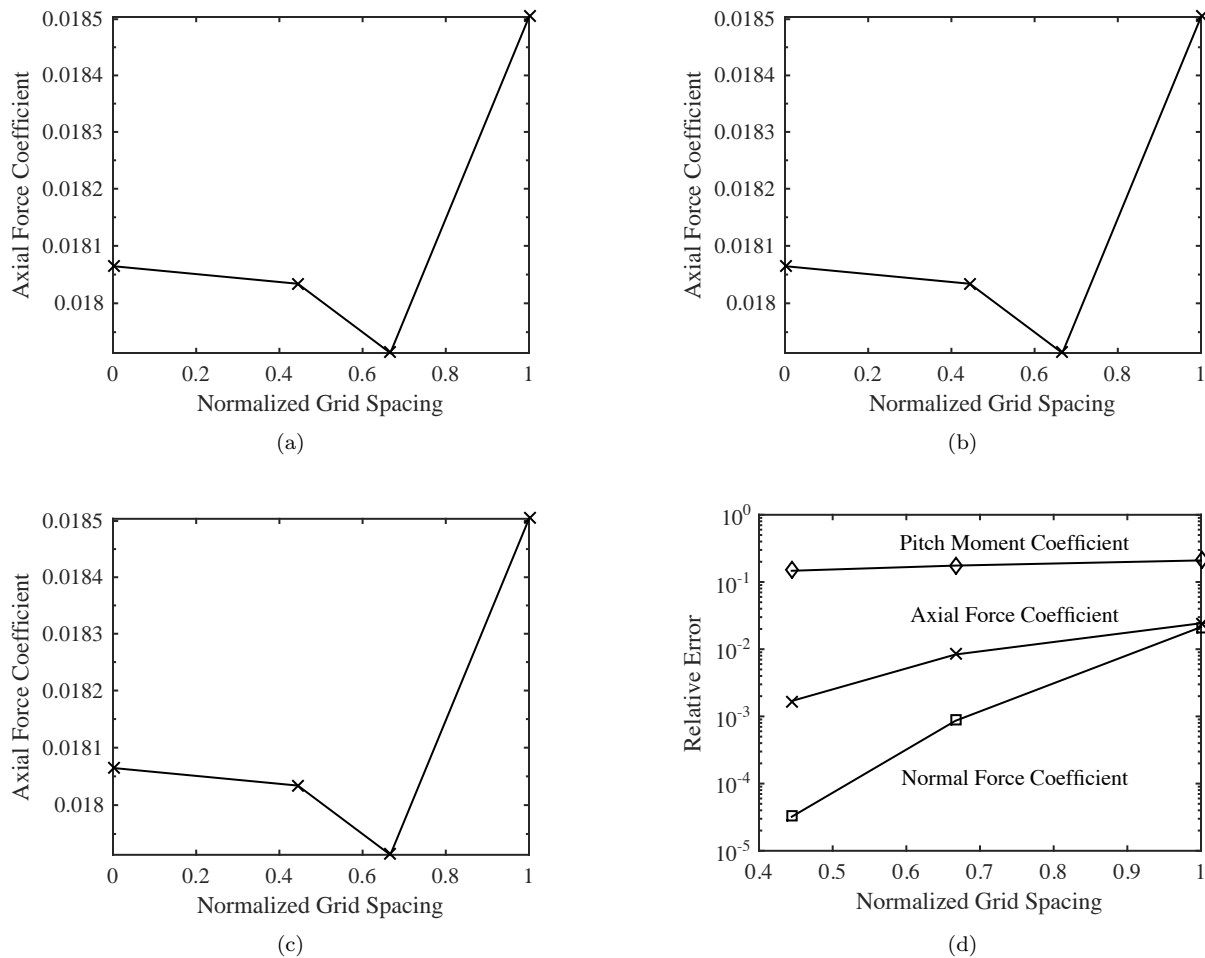
Figure 7. **Grid convergence results with the reference vehicle surface grid spacing approximately equal to** $L_{ref}/369$

with the attitude or divert jets on. The force and moment coefficients along with the respective amplification factors are presented in Figure 11. The results show that the jet interaction is not significantly affected by positive tip deflection with amplification factors approaching 1. However, the negative tip deflection causes a reduction in the force amplification due to a larger expansion region downstream of the jet and slight increase in the moment amplification factor for the attitude jet due to a larger boundary layer separation region upstream of the jet. In addition, the jet interaction due to the divert jets increases the moment coefficient for all levels of deformation due to the upstream boundary layer separation ahead of the center of gravity combined with the expansion region behind the center of gravity. This effect is larger for negative deformations that place more of the vehicle surface in the expansion region.

B.   Development of the Jet Interaction Model

The verification of the semi-empirical and data-fusion jet interaction models is discussed next. The semi-empirical model is verified against previous numerical and experimental work using flat plates. Afterwards, the verification of the data-fusion model using a leave-one-out cross validation approach is presented.

1.   Semi-Empirical Jet Interaction Model Verification

The semi-empirical JI model was developed based on flat plate studies and the pressure distribution in the flow direction with a correction to account for three-dimensional effects. The flat plate solutions presented by DeSpirito[4] are used to verify the implementation of the model. The flat plate test case flow and jet

American Institute of Aeronautics and Astronautics

(a) AoA -45 deg, Attitude Jet On

(b) AoA 45 deg, Attitude Jet On

(c) AoA -45 deg, Divert Jets On
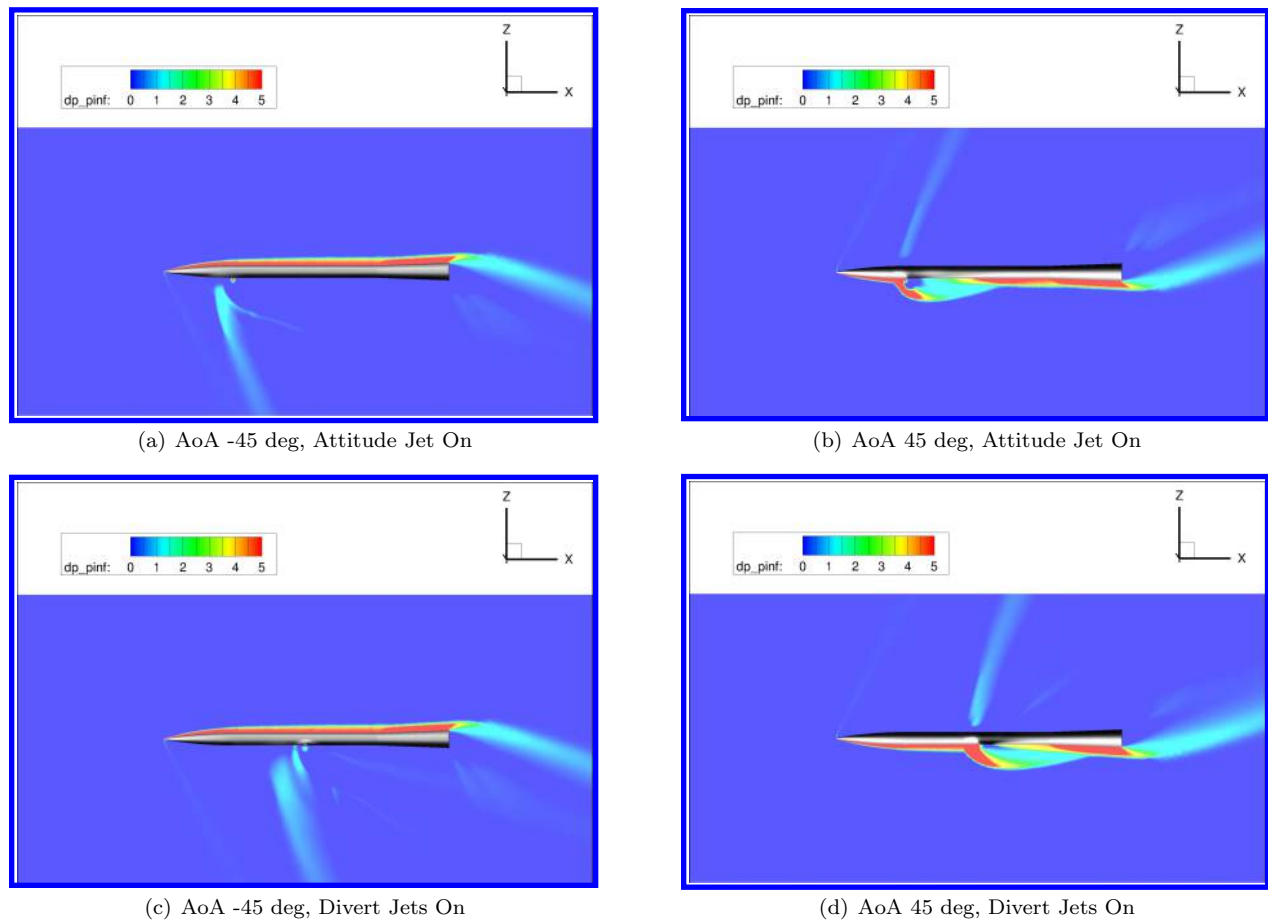
(d) AoA 45 deg, Divert Jets On

Figure 8. Contours of $\frac{p-p_\infty}{p_\infty}$ at Mach 3, 50,000 ft, and jet pressure ratio (PR) of 1500 with varying angles of attack.

parameters are listed in Table 4 for two test cases. These two test cases were chosen as a low-PR and high-PR case to test the range of applicability of the semi-empirical JI model.

Table 4. Test conditions of the flat plate with jet in supersonic cross-flow

	M_∞	p_∞, kPa	T_∞, K	T_{0j}, K	PR
Test 1	2.01	18.8	131	296	75.5
Test 2	2.61	6.73	133	296	308

DeSpirito[4] compared the computational results with various turbulence models to an experimental result. The semi-empirical model is compared in Figures 12 and 13 to the experimental pressure distribution and the computational solution calculated with the Spalart–Allmaras by DeSpirito.[4]

The semi-empirical JI model is able to capture the general locations of the various flow features, but the magnitudes are different. In the stream-wise direction, the lack of information immediately behind the jet results in an over-prediction of the surface pressure and the boundary layer separation point is miscalculated for the high PR condition. In the transverse direction, the shock location is generally well estimated by the model but the pressure at the shock boundary and the pressure distribution outside the shock is not well represented. Overall, the semi-empirical JI model represents a basic understanding of the problem but needs to be further refined using additional data from CFD or experiments.
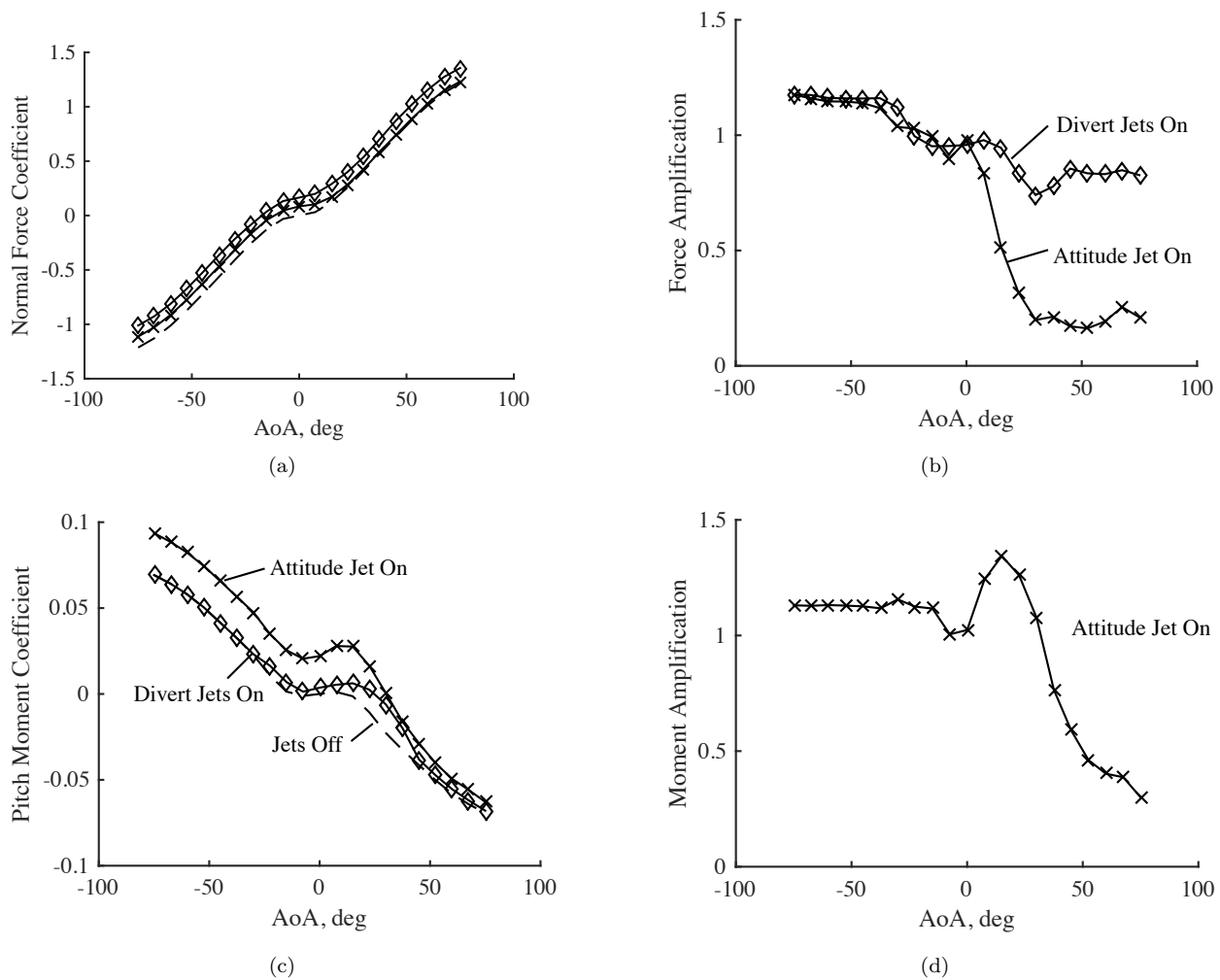
Figure 9. Force coefficients and the amplification factors due to jet interaction with varying angles of attack and no structural deformation. Flight conditions: Mach 3, 50,000 ft. Jet Conditions: PR 1500. (dashed) Jets Off, (×) Attitude Jet On, (◇) Divert Jets On.

2. Data-Fusion Jet Interaction Model Verification

The CFD solutions of the jet interaction, aerodynamic-only approximations from the surrogate model, and semi-empirical solutions of the jet interaction are used to build a co-Kriging model according to the procedure detailed in Section II. A cross validation was done to measure the quality of the data-fusion model by creating the data-fusion model without one of the CFD solutions and then measuring the error between the predicted solution at that point and the known CFD solution.[18] This leave-one-out process is repeated for every training point and avoids additional CFD runs for measuring model quality. For each high-fidelity test condition the surface pressure L_2 error norm, applied force error, applied moment error, and generalized force error were calculated and then normalized by the values associated with the validation point. The 95% confidence interval of the median for each error metric is presented in Table 5 calculated using bootstrap samples a total of 1000 times the number of leave-one-out evaluations. Each CFD solution used as training points and leave-one-out error calculation are independent, which is a critical assumption for cross validation analysis. The jet interaction model includes 1030 solutions across 5 dimensions and further sampling is expected to improve the accuracy of the model.
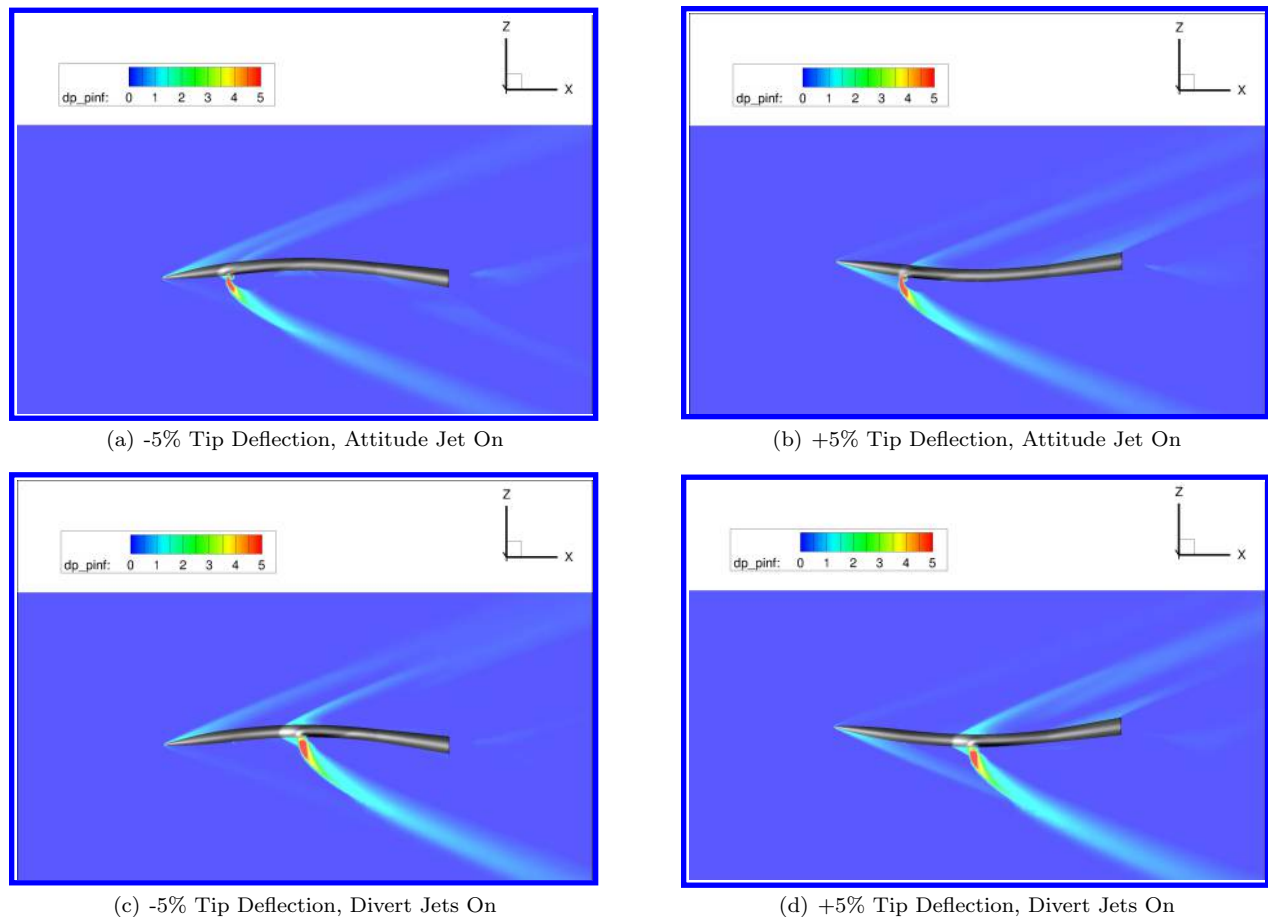
American Institute of Aeronautics and Astronautics

(a) -5% Tip Deflection, Attitude Jet On

(b) +5% Tip Deflection, Attitude Jet On

(c) -5% Tip Deflection, Divert Jets On

(d) +5% Tip Deflection, Divert Jets On

Figure 10. Contours of $\frac{p - p_\infty}{p_\infty}$ at Mach 3, 50,000 ft, and jet PR of 1500 with varying structural deformation

**Table 5. 95% confidence intervals of the median for the two surface pressure error metrics**

Error Metric	Lower Bound	Upper Bound
Normalized L_2-Norm	0.027	0.029
Applied Force Relative Error	0.061	0.073
Applied Moment Relative Error	0.113	0.139
Generalized Force Relative Error	0.036	0.045

V. Concluding Remarks

This paper focused on the fluid-structure-jet interaction (FSJI) problem of slender high-speed maneuverable vehicles with divert and attitude control jets. Specifically, the effect of vehicle deformation and high *AoAs* were studied because of the flexible structure and expected operating conditions of the vehicle. A FSJI loads prediction model was developed that leveraged pre-existing fluid-structure aerodynamic solutions of the vehicle and augmented them with additional high-fidelity CFD solutions of the jet interaction with vehicle deformation. The data-fusion technique known as co-Kriging was used to create a multi-fidelity model to converge to a FSJI model that could then be used within a flight simulation framework.

The change in vehicle loading to the fluid, structure, and jet parameters was determined by doing a set of parameter sweeps from the lower to upper bounds of each parameter. The range of *AoAs* of −75 to 75 degrees was used to study the effect of high *AoAs* on the jet interaction. The jet interaction at small *AoAs* has a positive effect, which would be helpful for initiating a maneuver from a small *AoA* or from the opposite direction (large negative *AoA*). At large positive *AoAs* with the jet on the windward surface the control

American Institute of Aeronautics and Astronautics
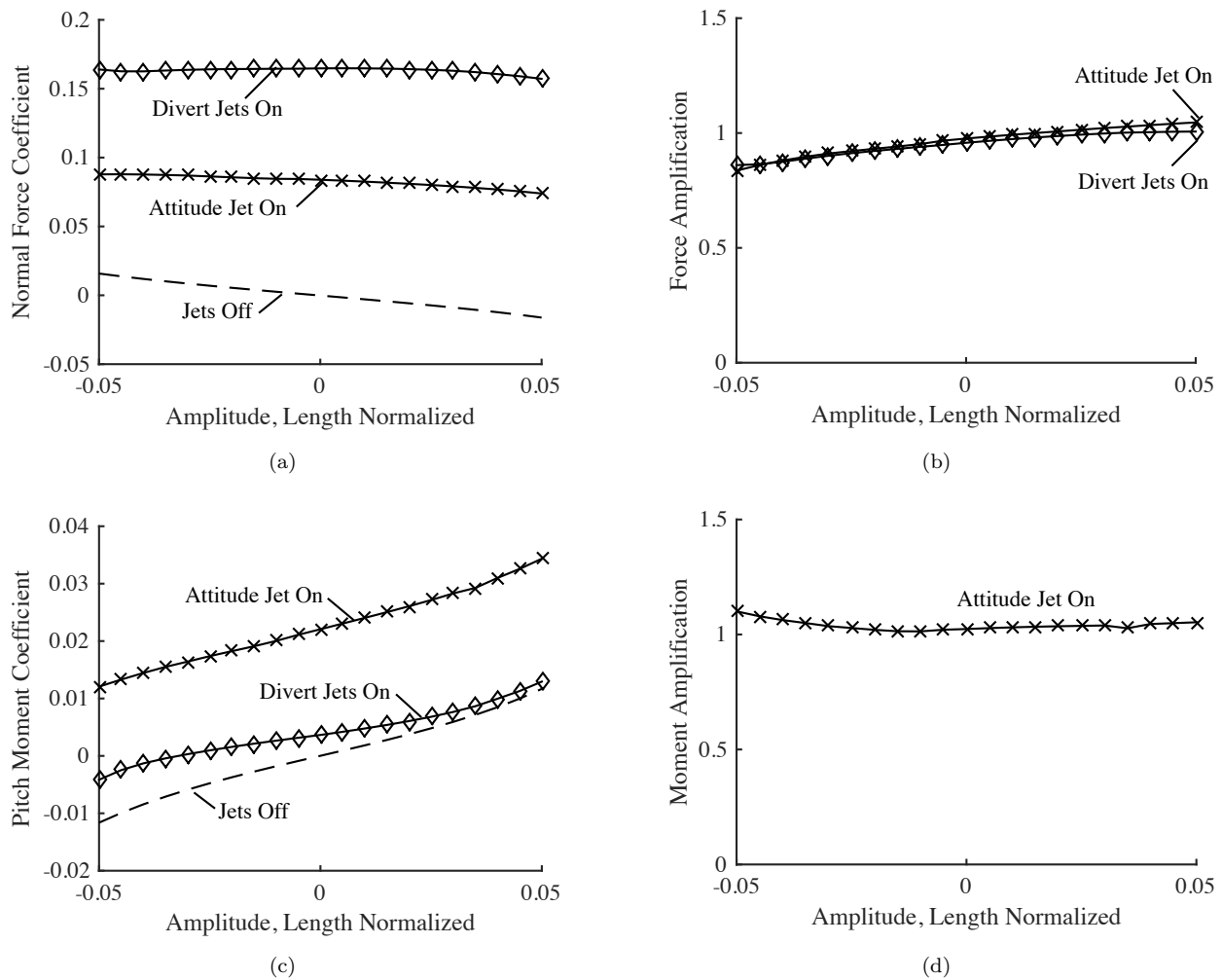
Figure 11. Force coefficients and the amplification factors due to jet interaction with varying tip deflection. Flight conditions: Mach 3, 50,000 ft. Jet Conditions: PR 1500. (_dashed_) Jets Off, ($\times$) Attitude Jet On, ($\diamond$) Divert Jets On.

effectiveness is significantly reduced by a large low pressure region that develops downstream of the jet as the flow expands turning around the jet flow. Therefore, the attitude jets become much less effective at high $AoAs$. The divert jets lose effectiveness at high $AoAs$, but not as significantly and could provide additional normal force to increase the vehicle acceleration.

The range of vehicle deformation from positive to negative 5% tip bending was studied to understand how vehicle deformation would affect the jet interaction. This is an important concept to understand for slender vehicles with increased flexibility that will deform under applied aerodynamic and jet loads. The primary effects of the jet interaction with a supersonic cross-flow that need to be taken into account are the boundary layer separation upstream of the jet, indicated by the flowfield features that causes a high-pressure region, and the expansion region due to the free-stream flow turning around the jet flow causing a low-pressure region just behind the jet. At zero AoA and negative tip deflection, the vehicle surface area within the low-pressure region is increased due to the attitude and divert jets, which results in the force amplification to be below 1, indicating a loss in control effectiveness. At positive tip deflections, this expansion region on the vehicle surface is reduced and the jet interaction amplifies the applied force due to the boundary layer separation. The moment amplification is approximately 1 over the range of tip deflections with a slight increase at negative tip deflections due to a larger boundary layer separation region upstream of the jet. These results are especially of note for the divert jet because the jet thrust would lead to a negative deformation and a reduced effectiveness. The attitude jet thrust would cause a positive deformation and

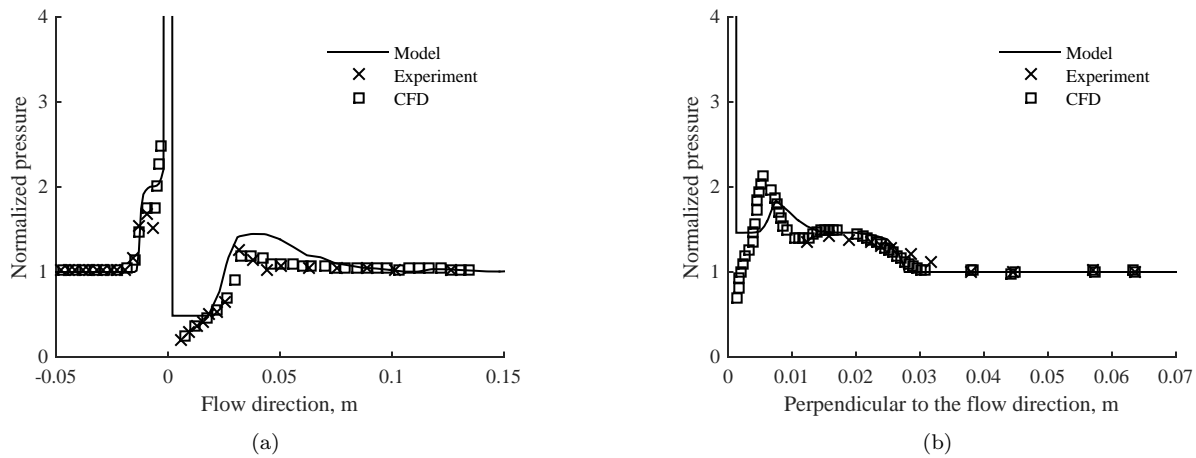American Institute of Aeronautics and Astronautics

Figure 12. Pressure distribution due to JI as calculated by the semi-empirical JI model ("Model"), computational ("CFD") and experimental results from the literature for test case 1 conditions.
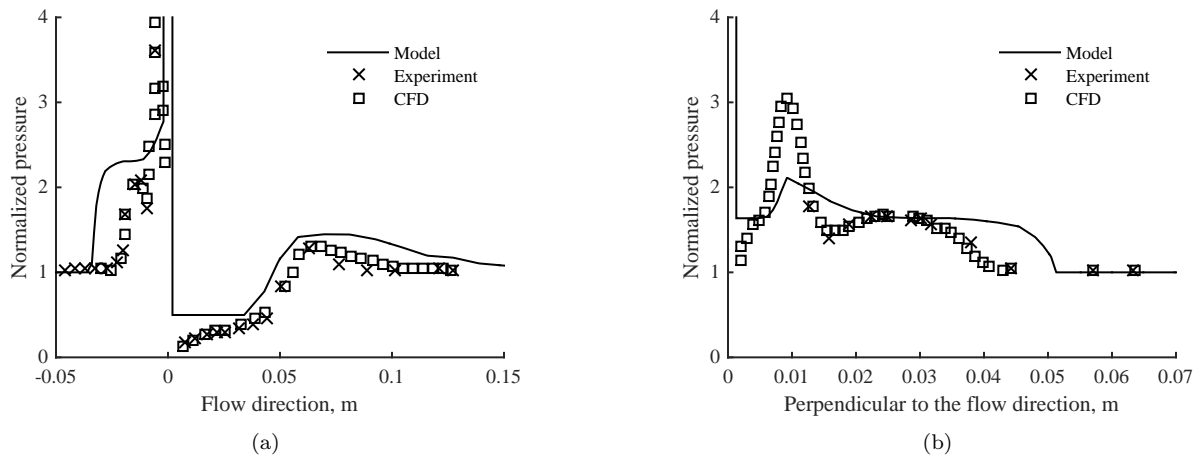

Figure 13. Pressure distribution due to JI as calculated by the semi-empirical JI model ("Model"), computational ("CFD") and experimental results from the literature for test case 1 conditions.

slightly increased force and moment effectiveness due to jet interaction.

A semi-empirical jet interaction model has been developed to get a first approximation to surface pressure due to a jet in supersonic cross-flow. The model was built on theoretical and empirical models in the literature and combined to get a three-dimensional approximation. The semi-empirical model was then compared to previous numerical and experimental flat plate studies with jets in supersonic cross-flow. The comparison shows that the model approximates the main jet interaction features such as boundary layer separation and shock locations, but the magnitudes may differ depending on the jet and flow conditions. However, this model is useful as an inexpensive solution to the jet interaction problem and can be combined with an aerodynamic surrogate model to approximate the surface pressure distribution over a complex geometry.

A FSJI model was created using semi-empirical and existing loads models with additional CFD solutions of the deformed representative high-speed vehicle with jet interaction. The semi-empirical JI model was combined with an existing CFD-based aerodynamic surrogate model for a representative high-speed vehicle to create a computationally inexpensive jet interaction model. The inexpensive solution was then combined with additional CFD solutions of the representative vehicle with jet interaction using a data-fusion technique. The data-fusion model is able to leverage the understanding of the inexpensive solution and augment the approximation with additional CFD solutions. The result is a model that approximates the computationally expensive jet interaction CFD solutions near the additional training points and regresses to the inexpensive

American Institute of Aeronautics and Astronautics
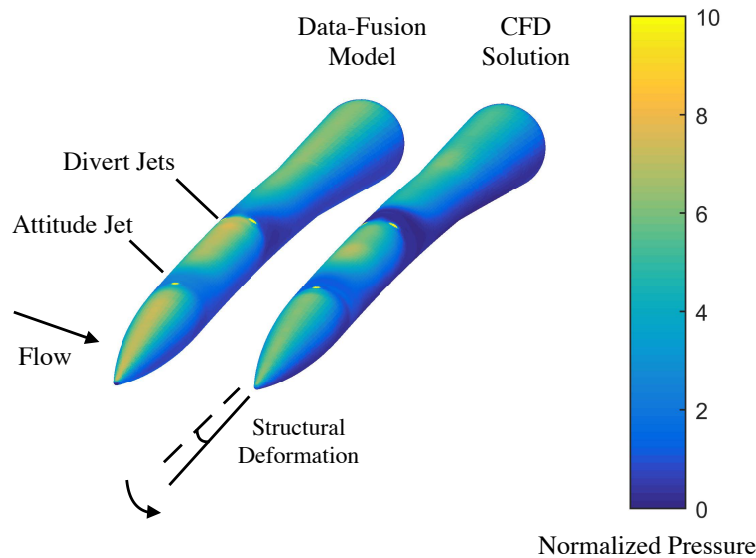
Figure 14. Surface pressure distribution of the data-fusion model and CFD solution. Input conditions: Mach 2.11, 68 deg flow incidence angle, 1% tip deflection, Attitude Jet PR 690, Divert Jets PR 1350

solution where there is no high-fidelity solution. The data-fusion technique was combined with a method of reducing the surface solution to a set of basis vectors, which reduced the size of the model. The model approaches the full CFD solution and may be used within a simulation framework to approximate the vehicle loading.

Overall, the introduction of very high $AoAs$ and structural deformations to the jet interaction with supersonic cross-flow problem reveals some insight that can be used for future work regarding modeling and simulation of high-speed vehicles with divert and attitude control jets. First, the AoA has a significant effect on the jet interaction and resultant loads, with a variation of -80% to $+40\%$ in control effectiveness. Second, moderate structural deformation had an impact on the jet interaction and resultant loads that was nonlinear about the zero deflection point with possible 15% reduction in control effectiveness. The jet interaction modeling methodology presented demonstrates how data-fusion techniques can be used to reduce the additional computational cost to converge to a new jet interaction model from a purely aerodynamic model. In addition, the surface domain decomposition techniques reduced the highly dimensional surface mesh into jet interaction mode shapes that further reduced the number of degrees of freedom that needed to be approximated by the jet interaction model. This work provides initial insight into the FSJI problem and a modeling methodology that can be built upon for further aeroelastic analysis of high-speed agile vehicles with jet interaction.

Acknowledgments

References

[1]Ebrahimi, H. B., "Numerical Simulation of Transient Jet-Interaction Phenomenology in a Supersonic Freestream," *Journal of Spacecraft and Rockets*, Vol. 37, No. 6, November–December 2000, pp. 713–719.

[2]Naumann, K. W., Ende, H., George, A., and Mathieu, G., "Stationary and Time-Dependent Effects in the Near Interaction of Gaseous Jets and Supersonic Cross-flow," *29th AIAA Fluid Dynamics Conference*, AIAA 1998-2972, 1998.

[3]Roger, R. P., "The Aerodynamics of Jet Thruster Control for Supersonic/Hypersonic Endo-Intercepters: Lessons Learned," *37th AIAA Aerospace Sciences Meeting and Exhibit*, AIAA 99-0804, January 1999.

American Institute of Aeronautics and Astronautics

[4]DeSpirito, J., "Factors Affecting Reaction Jet Interaction Effects on Projectiles," *29th AIAA Applied Aerodynamics Conference*, AIAA 2011-3031, June 2011.

[5]Ferrante, A., Matheou, G., and Dimotakis, P. E., "LES of an Inclined Jet into a Supersonic Turbulent Crossflow: Synthetic Inflow Conditions," *48th AIAA Aerospace Sciences Meeting Including the New Horizons Forum and Aerospace Exposition*, AIAA 2010-1287, January 2010.

[6]Werle, M. J., Driftmyer, R. T., and Shaffer, D. G., "Jet-Interaction-Induced Separation: The Two-Dimensional Problem," *AIAA Journal*, Vol. 10, No. 2, February 1972, pp. 188–193.

[7]Sakurai, A., "On the Propagation and Structure of the Blast Wave, I," *Journal of the Physical Society of Japan*, Vol. 8, No. 5, September–October 1953, pp. 662–669.

[8]Sakurai, A., "On the Propagation and Structure of the Blast Wave, II," *Journal of the Physical Society of Japan*, Vol. 9, No. 2, March–April 1954, pp. 256–266.

[9]Broadwell, J. E., "Analysis of the Fluid Mechanics of Secondary Injection for Thrust Vector Control," *AIAA Journal*, Vol. 1, No. 5, May 1963, pp. 1067–1075.

[10]Sahu, J., Fresconi, F., and Heavey, K. R., "Unsteady Aerodynamic Simulations of a Finned Projectile at a Supersonic Speed With Jet Interaction," Tech. Rep. ARL-TR-6960, U.S. Army Research Laboratory, Aberdeen Proving Ground, MD, June 2014.

[11]VanderWyst, A. S., Shelton, A. B., Martin, C. L., Neergaard, L. J., and Witeof, Z. D., "Reduced Order Models for Generation of Large, High Speed Aerodynamic Databases with Jet Interactions," *57th AIAA/ASCE/AHS/ASC Structures, Structural Dynamics and Materials Conference*, AIAA 2016-0464, January 2016.

[12]Forrester, A. I. J., Sóbester, A., and Keane, A. J., "Multi-fidelity optimization via surrogate modelling," *Proceedings of the Royal Society of London A: Mathematical, Physical and Engineering Sciences*, Vol. 463, No. 2088, 2007, pp. 3251–3269.

[13]Kennedy, M. C. and O'Hagan, A., "Predicting the output from a complex computer code when fast approximations are available," *Biometrika*, Vol. 87, No. 1, 2000, pp. 1–13.

[14]Zukoski, E. E., "TurbulentBoundar-Layer Separation in Front of a Forward-Facing Step," *AIAA Journal*, Vol. 5, No. 10, October 1967, pp. 1746–1753.

[15]Zettl, D., Dreyer, E. R., Grier, B. J., McNamara, J. J., and Pasiliao, C. L., "Rapid Steady-State Pressure Prediction for Ultra High-Speed Vehicles," *15th Dynamics Specialists Conference*, AIAA 2016-1323, 2016.

[16]Biedron, R. T., Carlson, J., Derlaga, J. M., Gnoffo, P. A., Hammond, D. P., Jones, W. T., Kleb, B., Lee-Rausch, E. M., Nielsen, E. J., Park, M. A., Rumsey, C. L., Thomas, J. L., and Wood, W. A., "FUN3D Manual 12.9," Tech. Rep. NASA-TM-2016-219012, NASA, 2016.

[17]Kitson, R. C. and Cesnik, C. E. S., "Aeroelastic Modeling and Simulation of High-Speed Flexible Vehicles," *15th Dynamics Specialists Conference*, AIAA 2016-1324, January 2016.

[18]Tinsley, H. E. A. and Brown, S. D., *Handbook of Applied Multivariate Statistics and Mathematical Modeling*, 2000, pp. 23–25.

American Institute of Aeronautics and Astronautics